 

# DC Fault Protection Structures at a DC-Link Node in a Radial Multi-Terminal HVDC System

Rui Li[1], John E Fletcher[2], Liangzhong Yao[3], and Barry W. Williams[1]

[1]Department of Electronic and Electrical Engineering, University of Strathclyde, Glasgow, UK

[2]School of Electrical Engineering and Telecommunications, University of New South Wales, Sydney, Australia

[3]China Electric Power Research Institute, Beijing, China

**E-mail:** rui.li@strath.ac.uk

***Abstract*—**In a multi-terminal HVDC system, DC circuit breakers (DCCBs) are conventionally connected in a star-configuration to enable isolation of a DC fault from the healthy system parts. However, a star-connection of DCCBs has disadvantages in terms of loss, capacity, reliability, etc. By rearranging the star-connection DCCBs, a novel delta-configuration of DCCBs is proposed in this paper. As each terminal is connected to each of the other terminals through only one DCCB, the current flows through only one DCCB when transferring power between any two terminals compared with two DCCBs in the current path for the conventional star-arrangement. The total loss of the proposed delta-configuration is only 33.3% of that of star-configuration, yielding a high efficiency. Also, any DC fault current is shared between two DCCBs instead of one DCCB in the faulty branch suffering the fault current. As a result, DCCB capacities in the proposed delta-configuration are only half those in a star-arrangement. Additionally, in the case of one or two DCCBs out of order, the power can still be transferred among three or two terminals, thereby affording high supply security of all HVDC links. Based on the DCCB delta-configuration, two novel DC fault protection structures with external and internal DC inductances are proposed. Their characteristics are discussed and it is shown a DC fault can be isolated using slow DCCBs without exposing any converter to significant over-current. The results demonstrate DC fault tolerant operation is achieved by using the proposed DC fault protection structures with delta-configuration.

***Index Terms*—DC fault protection, DC inductance, delta-configuration of DC circuit breakers, multi-terminal HVDC system, modular multilevel converter (MMC).**

 

## I. INTRODUCTION

One of the main development challenges of multi-terminal HVDC transmission systems is the protection and post-fault operation after a DC-link fault. In the event of a DC short-circuit, high current flows through the freewheel diodes in half-bridge (HB) based modular multilevel converters (MMCs) from the AC grid to the DC-link side [1]. DC circuit breakers are typically required to disconnect the MMC from the AC grid or DC fault point.

The potential DC circuit breaker (DCCB) technologies for multi-terminal HVDC systems include mechanical, solid-state, and hybrid DCCBs. The losses incurred in mechanical DCCBs are generally low as the breakers have a low equivalent contact resistance hence a low voltage drop across the circuit breaker element. Typically mechanical DCCB losses are negligible compared to the transmitted power. However conventional mechanical DCCB response is slow, whence semiconductors endure high current stress [2-4].

In [5], the solid-state DCCBs are connected at both ends of each cable and at station terminals, where service interruption can be avoided due to fast fault isolation. However, this is at the expense of high capital cost and significant on-state operational losses due to the semiconductors in the main current path. In order to reduce loss and cost, the solid-state DCCBs are only placed at the terminals of each station which disconnect the stations quickly from the faulty DC network [6]. However, the faulty cables have to be disconnected using DC switches and all the stations have to be temporarily shut down.

Hybrid DCCBs have been proposed where the mechanical path serves as the main conduction path with minimal loss during normal operation, and a parallel connected solid-state breaker is used for DC fault isolation [7, 8]. However, it has a relatively large footprint and its capital cost is high.

In [9], limiting reactors are connected with the fast acting DCCBs (e.g. solid-state DCCBs, hybrid DCCBs) to limit the fault current *di/dt* and decrease the fault current peak. However, all the system stations are blocked during the fault to avoid over-currents, causing shutdown of the entire multi-terminal HVDC system. In addition, there is no capacitor connected at the DC-link terminals with the MMC, thus the method is not viable.

In AC systems, the conduction losses of AC circuit breakers are generally low as AC breaker contacts have a low equivalent resistance hence a low voltage drop. Typically the power losses in an ACCB are negligible compared to the power transmitted through the circuit breaker. However, DC circuit breaker technology, particularly for high voltage systems, utilises new technologies, including solid-state circuit breakers where the semiconductors are used in the main current path. Thus the DC circuit breakers are sensitive to current stresses in terms of conduction losses, capital cost,

and volume.

The aim of this study is to use combinations of a novel DCCB arrangement and additional inductances on the DC line to reduce losses and capital costs and to improve system reliability, while ensuring continuous operation of the healthy parts in a multi-terminal HVDC system during a DC fault. The paper is organized as follows. The novel DCCB delta-configuration is proposed in Section II and its advantages over a conventional star-configuration are presented in detail. In Section III, protection structures combining delta DCCB configurations with DC inductances are introduced to isolate the DC fault and delay fault propagation through the healthy branches. DC fault tolerant operation with the proposed DC fault protection structures are assessed in Section IV, by considering a pole-to-pole DC fault at the DC-link node in a radial three-terminal HVDC system. Finally Section V draws the conclusions.

## II. Novel Delta-Configuration of DC Circuit Breakers

### *A. Radial Three-Terminal HVDC System*

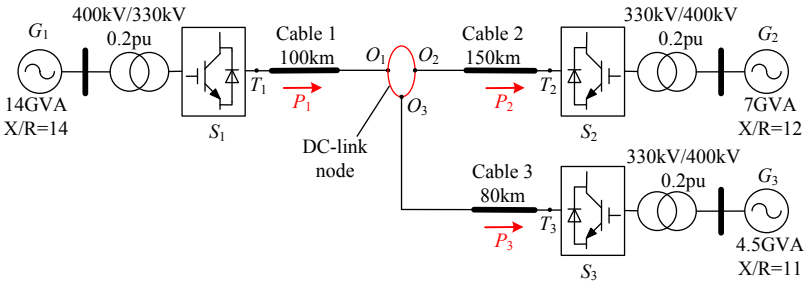


Fig. 1. Radial three-terminal HVDC transmission system.

TABLE I
Nominal Parameters of the Modelled System.

| Parameter | Nominal value |
|---|---|
| DC-link voltage | ±320 kV |
| SM number per arm | 304 |
| SM capacitor voltage | 2.1 kV |
| SM capacitance of stations $S_1$, $S_2$, and $S_3$ | 9.7 mF, 5.8 mF, 4.3 mF |
| arm inductance | 0.05 pu |
| pi section number of DC cable | 10 |
| DC cable resistance | 10 mΩ/km |
| DC cable inductance | 0.5 mH/km |
| DC cable capacitance | 0.27 μF/km |

Fig. 1 shows the basic radial three-terminal HVDC system being studied, where the stations are modelled as conventional HB submodule (SM) based MMCs using average models. The detailed parameters are listed in Table I. Station $S_1$ regulates the network DC voltage, with unity input power factor, while $S_2$ and $S_3$ inject rated active powers $P_2$

and $P_3$ into the AC grids $G_2$ and $G_3$, at unity power factors. Due to the large number of cell, the MMC is usually simplified to an average model for system-level analysis, to reduce the computation time. The average model has been validated as an effective approach to simulate the MMC behaviour and is widely used in MMC research, as demonstrated in [10, 11]. To improve simulation accuracy, each cable in this paper is modelled with 10 pi sections [8, 12, 13].

### *B. DC Circuit Breaker Arrangements*

Fig. 2 (a) shows the conventional DC circuit breaker configuration [5, 14-16]. The DCCBs $B_1$, $B_2$ and $B_3$ are connected in star-configuration and the other ends of $B_1$, $B_2$ and $B_3$ are connected with the terminals $O_1$, $O_2$ and $O_3$ in Fig. 1 respectively. Assuming the DC fault is applied across Cable 3, the corresponding breaker $B_3$ is commanded to open once the fault is detected. The DCCBs connecting the healthy branches remain closed to transfer power continuously. However, prior to the fault, the power transfer between any two terminals must pass through two series circuit breakers. Also, the DCCB on-state loss is high, especially for the solid-state circuit breakers. Thus it is beneficial to reduce the DCCB number in the main power path and lower the equivalent resistance of DCCBs between any two terminals.

In the event of a DC fault, the DCCB $B_3$ near the fault location cannot be opened immediately and time is needed for the DCCB to act. Hence all the DCCBs suffer fault currents before the fault is isolated, especially circuit breaker $B_3$ in the faulted branch. As $B_3$ is near the fault, it suffers the sum of the fault currents via the other (two) DCCBs, $i_{Yf1}$+$i_{Yf2}$ in Fig. 2 (a). Hence DCCB capacities have to be large to tolerant the fault current from multiple paths, resulting in high capital cost and loss. Also since each fault current path from each link involves two series DCCB, series breaker discrimination is an issue.

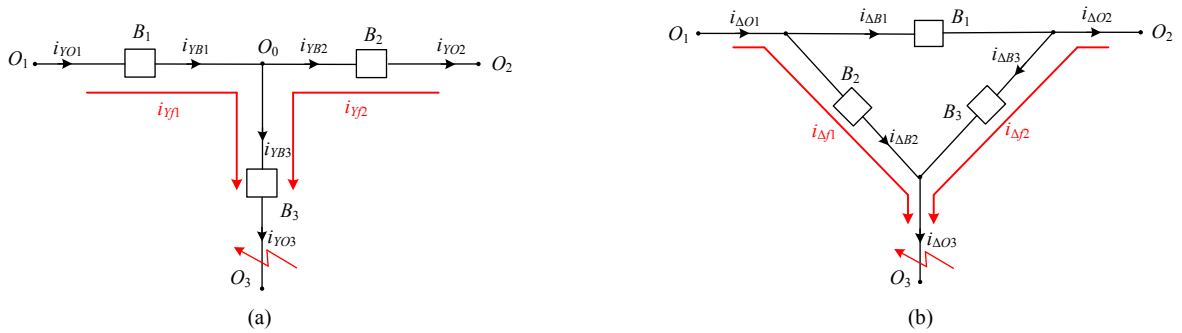


Fig. 2. DC circuit breaker configurations: (a) conventional star-configuration and (b) proposed delta-configuration.

To solve the accumulating current problem of the basic star DCCB configuration, a novel DCCB connection is proposed, Fig. 2 (b). The three breakers $B_1$, $B_2$ and $B_3$ are connected in a delta-configuration to the three terminals $O_1$, $O_2$ and $O_3$ in Fig. 1. When a DC fault occurs, the protection system activates the appropriate set of DCCBs to isolate the

fault. The two DCCBs connected to the faulted link are opened, with one DCCB remaining connected between the two healthy branches. Since the DCCBs are not series connected, discrimination is not an issue. In Fig. 2 (b), currents flow through only one circuit breaker to transfer power between any two terminals thus low losses are expected for the proposed delta-configuration. Moreover, only two DCCBs suffer fault currents while the other does not experience over-current. Additionally, the proposed delta DCCB configuration provides other technical benefits, such as high reliability and low capacity, which are addressed in the following parts.

Two breakers in the delta-configuration need to be opened to isolate a fault, rather than one breaker in the star-connection. This potentially has a negative influence on reliability, when considering DCCB failure. However, remote back-up, as is standard practice, provides ultimate backup protection. In the event of a breaker failure, i.e. a circuit breaker fails to interrupt the fault current, system backup has to be activated before the rising fault current exceeds the interrupting capacity of the system section [17-19]. Since this may involve AC breakers taking station off line, section of the system may be temporarily lost while mechanical isolators are activated.

The proposed delta-configuration does not depend on the detailed realisation of the DCCB. All the mechanical, hybrid, and solid-state DCCBs can be in the delta-configuration. For simplicity, the DCCB used in this study is modelled as a mechanical switch with an opening time of 10 ms and a metal-oxide surge arrester is shunt connected with each mechanical switch to absorb the DC line energy and to protect the DCCB against over-voltages [20]. The detailed DCCB model in the MATLAB/Simulink® environment shown in Fig. 3 is used in this paper. The mechanical switch is represented by an ideal switch $S_w$ in series with an on-state resistance $R_B$, which are connected in parallel with a series $RC$ snubber circuit (resistor $R_{Sn}$ and capacitor $C_{Sn}$). The switch $S_w$ is controlled by a gate signal, and has an on-state resistance $R_B$ while the off-state resistance is infinite. The metal-oxide surge arrestor is modelled as a physical model as shown in [21] where the non-liner resistance $A_0$ is paralleled with the leakage resistance $R_{Pmo}$ and parasitic capacitance $C_{Pmo}$ and then is series connected with resistance $R_{Smo}$ and inductance $L_{Smo}$. The DCCB model provides enough detail for the studies performed in this paper.

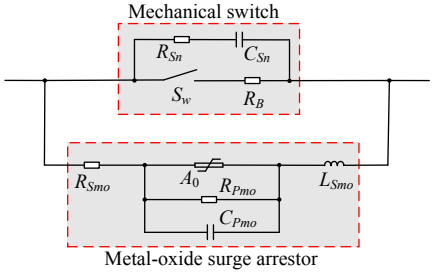


Fig. 3. Detailed model of DC circuit breaker where the metal-oxide surge arrestor is modelled as the physical model, as in [21].

 

### C. *Efficiency Consideration*

#### 1) *During normal operation*

A key technical advantage of the proposed delta-configuration is that currents need only flow through one circuit breaker in order to transfer power between terminals compared with having to flow through two breakers when using prior art. In Fig. 2 (a), the current equation of the star DCCB configuration is:

$$i_{YO1} - i_{YO2} - i_{YO3} = 0. \tag{1}$$

As all the DC circuit breakers are modelled with conduction resistance $R_B$, the power loss of the star-configuration is:

$$P_Y = {i_{YO1}}^2 R_B + {i_{YO2}}^2 R_B + {i_{YO3}}^2 R_B = 2R_B\left({i_{YO2}}^2 + {i_{YO3}}^2 + i_{YO2} i_{YO3}\right). \tag{2}$$

For the proposed delta DCCB configuration, Fig. 2 (b), low conduction losses are expected as the current can transit from one terminal to another terminal through parallel paths. According to the Kirchhoff's current law, the current equations are:

$$i_{\Delta O1} - i_{\Delta O2} - i_{\Delta O3} = 0 \tag{3}$$

$$i_{\Delta B2} + i_{\Delta B3} - i_{\Delta O3} = 0 \tag{4}$$

$$i_{\Delta B1} - i_{\Delta B3} - i_{\Delta O2} = 0. \tag{5}$$

Also, the voltage equation of delta-configuration is expressed as:

$$i_{\Delta B1} R_B - i_{\Delta B2} R_B + i_{\Delta B3} R_B = 0. \tag{6}$$

According to (3)-(6), the power loss of the delta-configuration is:

$$P_\Delta = {i_{\Delta B1}}^2 R_B + {i_{\Delta B2}}^2 R_B + {i_{\Delta B3}}^2 R_B = \frac{2R_B}{3}\left({i_{\Delta O2}}^2 + {i_{\Delta O3}}^2 + i_{\Delta O2} i_{\Delta O3}\right). \tag{7}$$

The different DCCB structures shown in Fig. 2 only influence the currents through the circuit breakers, while the terminal currents at $O_1$, $O_2$ and $O_2$ are independent with the DCCB configurations and can be described by

$$i_{\Delta O1} = i_{YO1} = i_{O1}, \qquad i_{\Delta O2} = i_{YO2} = i_{O2}, \qquad i_{\Delta O3} = i_{YO3} = i_{O3}. \tag{8}$$

As a result, the power loss of delta DCCB configuration is only a third that of star-configuration and high efficiency is expected for the proposed delta-configuration:

$$P_\Delta = \frac{2R_B}{3}\left({i_{O2}}^2 + {i_{O3}}^2 + i_{O2} i_{O3}\right) = \frac{P_Y}{3}. \tag{9}$$

The loss estimate is comparative, whether the on-state resistance is because of semiconductors or other potential breaker technologies. It does not depend on DCCB type and the conduction losses of all DCCB types are reduced to 33.3% that of the star-configuration. This is more important for the solid-state DCCB, which is an

 

option for DC fault protection of VSC HVDC systems [22, 23] but suffers high conduction losses. Due to the significant reduction of conduction losses, the delta-configuration makes solid-state breakers more viable for future DC grids, especially in an application where limited fault current rise time and fast DC fault blocking capability are a high priority.

The on-state resistance of a mechanical DCCB is low and the incurred conduction losses are insignificant compared to the transmitted power through the circuit breaker. However, due to the auxiliary semiconductor based DC breaker in the main current path, the on-state resistance of the hybrid DCCB proposed by ABB in [24-26] cannot be ignored and a forced cooling system is required. By using the proposed delta DCCB configuration, the cooling system requirements can be reduced.

*2) Post-fault operation*

After the DC fault, the faulted branch is isolated from the multi-terminal HVDC system by the corresponding circuit breaker(s) while power can still be transferred between the healthy branches. With the basic star DCCB configuration, the current flows through two circuit breakers. But the current only needs to flow through one circuit breaker for the delta DCCB configuration. As a result, in post-fault operation, the power loss of the proposed DCCB structure is only half of that of the star-configuration:

$$P_{\Delta} = \tfrac{1}{2} P_{Y}. \tag{10}$$

*D. Energy Supply Security*

By using the proposed delta DCCB configuration, the energy supply security can be dramatically enhanced. If a circuit breaker is out of service in the star-configuration, the link terminal connecting the fault DCCB has to be isolated and the HVDC transmission system loses the corresponding power capability. This means that one DCCB out-of-service in the prior art scheme results in only one of three power flow paths being available. On the other hand, power can still be transferred between all three-terminals through the remaining healthy circuit breakers, in the event of any one DCCB being out of service, benefiting from the parallel current paths in the delta connection configuration. Therefore the proposed delta-configuration is tolerant to any circuit breaker being out of service, yielding high reliability. The power capacities that could be transferred among the stations are dependent on the power capacities of the healthy DCCBs. Power flow limitations may be necessary but all three power flow paths can be utilized with one DCCB out of service, as shown in Fig. 4 (a). When two DCCBs in star-configuration are out of service, it is impossible to transfer any power as all the stations are isolated from each other. But with the delta-configuration power can still be transferred between

 

the two terminals that are connected through the healthy DCCB, as demonstrated in Fig. 4 (b).

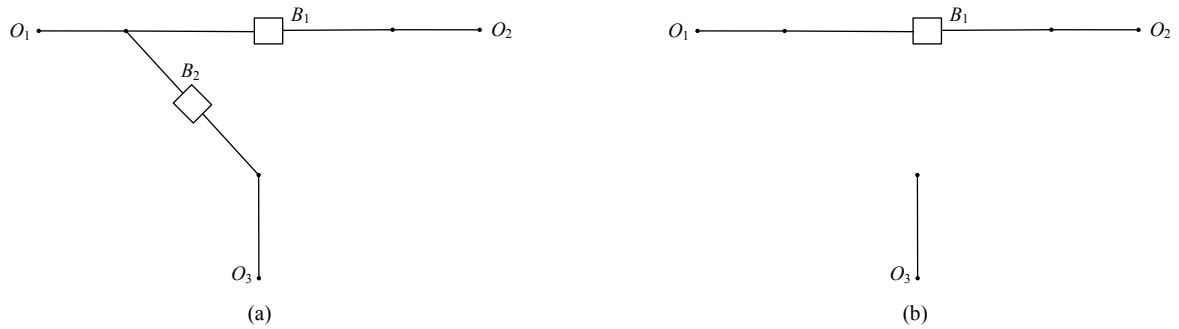


Fig. 4. Delta DCCB configurations with one (a) or two (b) DCCBs out of service.

## III. DC Fault Protection Structures at DC-Link Node

### *A. DC Fault Protection Structures with DC Inductances*

To reduce the fault propagation and limit the current rise, DC fault protection structure with star-configuration is presented in [27] as shown in Fig. 5, where an additional DC inductance (DCL) is connected in series with each circuit breaker in Fig. 2 (a). However, as the DCCBs are connected in a star-configuration, the losses, capacity, and reliability of this protection structure are not optimized and the performance can be improved by using the proposed delta-connection of DCCBs.

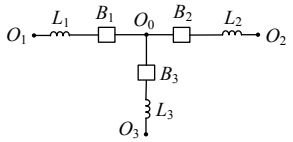


Fig. 5. Star-configuration with DCLs, presented in [27].


Fig. 6. Proposed DC fault protection structures: (a) delta-configuration with external DCLs and (b) delta-configuration with internal DCLs.

Two DC fault protection structures are proposed in this section to effectively utilize the advantages of the delta-configuration over the star connection. By connecting a DC inductor at each terminal of the proposed delta-configured DCCBs, the external DCL arrangement is as shown in Fig. 6 (a). The relatively slow circuit breakers are used to isolate the fault while DC inductors prolong the fault propagation. The added inductor is particularly effective, when the pole-to-pole DC fault is applied at the DC-link node, preventing the DC-link node voltage dropping to zero immediately. This

will allow continued power transfer and avoid shutdown of the entire radial multi-terminal system.

Compared with the external DCCB structure in Fig. 6 (a), the inductors in Fig. 6 (b) are located inside the delta structure. As a result, the current stresses on internal inductors are lower and DCCB currents cannot change discontinuously.

The proposed protection structures do not depend on the detailed realisation of the DCCB. Apart from mechanical DCCBs, other types of DCCBs, for example, the hybrid DCCB, can also be used in this study. If faster DCCB is used, the required additional DC inductance in the protection structure can be reduced significantly (discussed in Section IV B). Thus only the opening time of DCCB is critical to this study. This assumption has been used in [9], where the solid-state and hybrid DCCBs were both modelled as ideal switches and the difference is only the opening times.

### *B. Current Stresses on DC Circuit Breakers*

The simulated scenario assumes the system shown in Fig. 1 is subjected to the permanent pole-to-pole DC fault between the connection point $O_3$ and the Cable 3, which is the most serious fault position for the continuous operation of stations $S_1$ and $S_2$, at $t_0$=1 s. The station $S_3$ is blocked after the fault is detected while $S_1$ and $S_2$ continue to operate with maximum arm current threshold of 4 kA [28]. The fault detection and performance of $S_3$ are not within the scope of this paper and only the DC fault tolerant operation of the healthy parts (stations $S_1$ and $S_2$) is considered.

The currents through the DCCBs are illustrated in Fig. 7 and Table II. Prior to the fault, circuit breaker $B_1$ in star-configuration experiences the highest current stress, which is the sum of that through $B_2$ and $B_3$, Fig. 7 (a). On steady-state, the inductor voltage drops are zero thus the DCCB currents of delta-configurations with external and internal DCLs are identical. The currents are shared among the three circuit breakers and are much smaller than those of a star-configuration:

$$i_{\Delta B1}=\frac{i_{O1}+i_{O2}}{3},\qquad i_{\Delta B2}=\frac{2i_{O1}-i_{O2}}{3},\qquad i_{\Delta B3}=\frac{i_{O1}-2i_{O2}}{3}. \tag{11}$$

As the DCCBs are modelled with fixed on-state resistances ($R_B$) and the inductor losses are relatively small compared with DCCB losses, the total conduction losses of the DC fault protection structures on normal operation are

$$P_Y=P_{YB1}+P_{YB2}+P_{YB3}=(1960\text{A})^2R_B+(1130\text{A})^2R_B+(830\text{A})^2R_B=5807400\text{A}^2R_B \tag{12}$$

$$P_\Delta=P_{\Delta B1}+P_{\Delta B2}+P_{\Delta B3}=(1030\text{A})^2R_B+(930\text{A})^2R_B+(100\text{A})^2R_B=1935800\text{A}^2R_B. \tag{13}$$

The total loss of delta-configuration is 33.3% of that of the star-configuration and is in agreement with (9):

$$\frac{P_\Delta}{P_Y}=\frac{1935800\text{A}^2R_B}{5807400\text{A}^2R_B}=33.3\%. \tag{14}$$

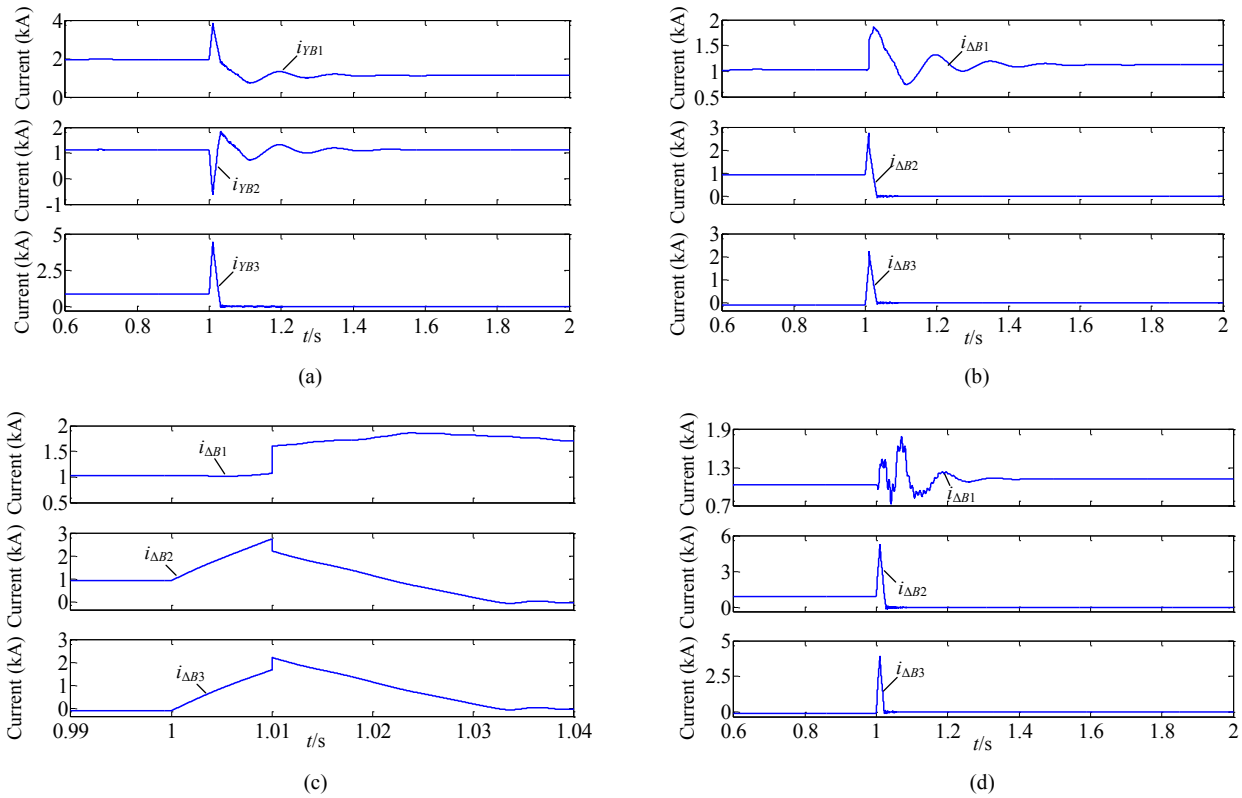


Fig. 7. Currents of DC circuit breakers $B_1$, $B_2$, and $B_3$: (a) star-configuration with DCLs, (b) delta-configuration with external DCLs, (c) details of (b), and (d) delta-configuration with internal DCLs.

After the fault, the station $S_3$ is isolated from the HVDC system and the current $i_{O3}$ drops to zero eventually. On the post-fault steady state, the total conduction losses of the DC fault protection structures are

$$P_Y = P_{YB1} + P_{YB2} + P_{YB3} = (1120\text{A})^2 R_B + (1120\text{A})^2 R_B + (0\text{A})^2 R_B = 2508800\text{A}^2 R_B \tag{15}$$

$$P_\Delta = P_{\Delta B1} + P_{\Delta B2} + P_{\Delta B3} = (1120\text{A})^2 R_B + (0\text{A})^2 R_B + (0\text{A})^2 R_B = 1254400\text{A}^2 R_B. \tag{16}$$

The total loss of delta-configuration is only 50% that of the star-configuration, which confirms (10):

$$\frac{P_\Delta}{P_Y} = \frac{1254400\text{A}^2 R_B}{2508800\text{A}^2 R_B} = 50\%. \tag{17}$$

In the star-configuration, the current $i_{YB1}$ increases while $i_{YB2}$ reverses into the fault at $t_0$=1 s and reach peaks of 3800 A and -600 A respectively at $t_1$=1.01 s. DCCB $B_3$ experiences the highest fault current, of 4400 A, which is the sum of currents $i_{YB1}$ and -$i_{YB2}$.

For the delta-arrangement with external DCLs, the inductors $L_1$ and $L_2$ suffer the same voltages but in opposite directions, at the fault initiation. As a result, the following equations are derived according to (11)

$$\frac{di_{\Delta B1}}{dt}(t_0) = 0, \qquad \frac{di_{\Delta B2}}{dt}(t_0) = \frac{di_{\Delta B3}}{dt}(t_0) = \frac{V_{DC}}{6L}. \tag{18}$$

During the fault (1 s-1.01 s), breaker $B_1$ does not suffer fault current but the currents through $B_2$ and $B_3$ increase, as shown in Fig. 7 (b) and (c) and Table II. Additionally, the maximum fault current peak of DCCBs is only 2730 A, much

 

lower than the star-configuration (4400 A). Thus the DCCB capacity of delta-arrangement with external DCLs is lower, yielding low power loss and cost. Following the opening of DCCBs $B_2$ and $B_3$ at $t_1$=1.01 s, part of current $i_{\Delta B2}$ is commutated to $B_1$ and $B_3$ to share the current $i_{\Delta O3}$ equally between $B_2$ and $B_3$, as $i_{\Delta B2}$ and $i_{\Delta B3}$ are commutated to the surge arrestors paralleled with the switches. Thus the DCCB currents at $t_1$=1.01 s are described as

$$i_{\Delta B2}(t_{1+}) = i_{\Delta B3}(t_{1+}) = \tfrac{1}{2} i_{\Delta O3}(t_1) \tag{19}$$

$$i_{\Delta B1}(t_{1+}) - i_{\Delta B1}(t_{1-}) = -\left[i_{\Delta B2}(t_{1+}) - i_{\Delta B2}(t_{1-})\right] = i_{\Delta B3}(t_{1+}) - i_{\Delta B3}(t_{1-}) \neq 0. \tag{20}$$

It can be seen from (20) that, following DCCB opening, the currents $i_{\Delta B1}$, $i_{\Delta B2}$ and $i_{\Delta B3}$ of delta-configuration with external inductors change discontinuously. Conversely, with the inductors located internally, the DCCB currents change continuously, Fig. 7 (d).

TABLE II
Current Stresses of Alternate DCCB Configurations with DC Inductances.

| LOCATION | CONFIGURATION | Pre-fault steady-state DC current (0 s-1 s) A | DC current peak during fault (1 s-1.01 s) A | Post-fault steady-state DC current (1.01 s-2 s) A | Arm current peak (0 s-2 s) A | AC side current peak (0 s-2 s) A |
|---|---|---|---|---|---|---|
| DC circuit breaker $B_1$ | Star with DCLs | 1960 | 3800 | 1120 | | |
| | Delta with external DCLs | 1030 | 1060 | 1120 | | |
| | Delta with internal DCLs | 1030 | 1330 | 1120 | | |
| DC circuit breaker $B_2$ | Star with DCLs | 1130 | -600 | 1120 | | |
| | Delta with external DCLs | 930 | 2730 | 0 | | |
| | Delta with internal DCLs | 930 | 5230 | 0 | | |
| DC circuit breaker $B_3$ | Star with DCLs | 830 | 4400 | 0 | | |
| | Delta with external DCLs | -100 | 1670 | 0 | | |
| | Delta with internal DCLs | -100 | 3900 | 0 | | |
| Station $S_1$ | Star with DCLs | | | | -3370 | -3420 |
| | Delta with external DCLs | | | | -3370 | -3420 |
| | Delta with internal DCLs | | | | -5240 | -3680 |
| Station $S_2$ | Star with DCLs | | | | 1830 | 1740 |
| | Delta with external DCLs | | | | 1830 | 1740 |
| | Delta with internal DCLs | | | | -3540 | 1740 |

For the star and delta DCCB arrangements with 500 mH external inductors, the arm current peaks are less than the threshold 4 kA and DC fault toleration operation is achieved. Additionally, stations $S_1$ and $S_2$ show the same performance and their arm currents are identical, which implies the proposed DCCB delta-configuration does not influence station performance. However, for the delta-configuration with 500 mH internal inductors, the switching device currents are higher than the threshold, due to the low short-circuit resistances at the DC-link node. To operate the healthy parts continuously, the internal inductances have to be increased.

### C. Energies Absorbed by Surge Arrestors in DC Circuit Breakers

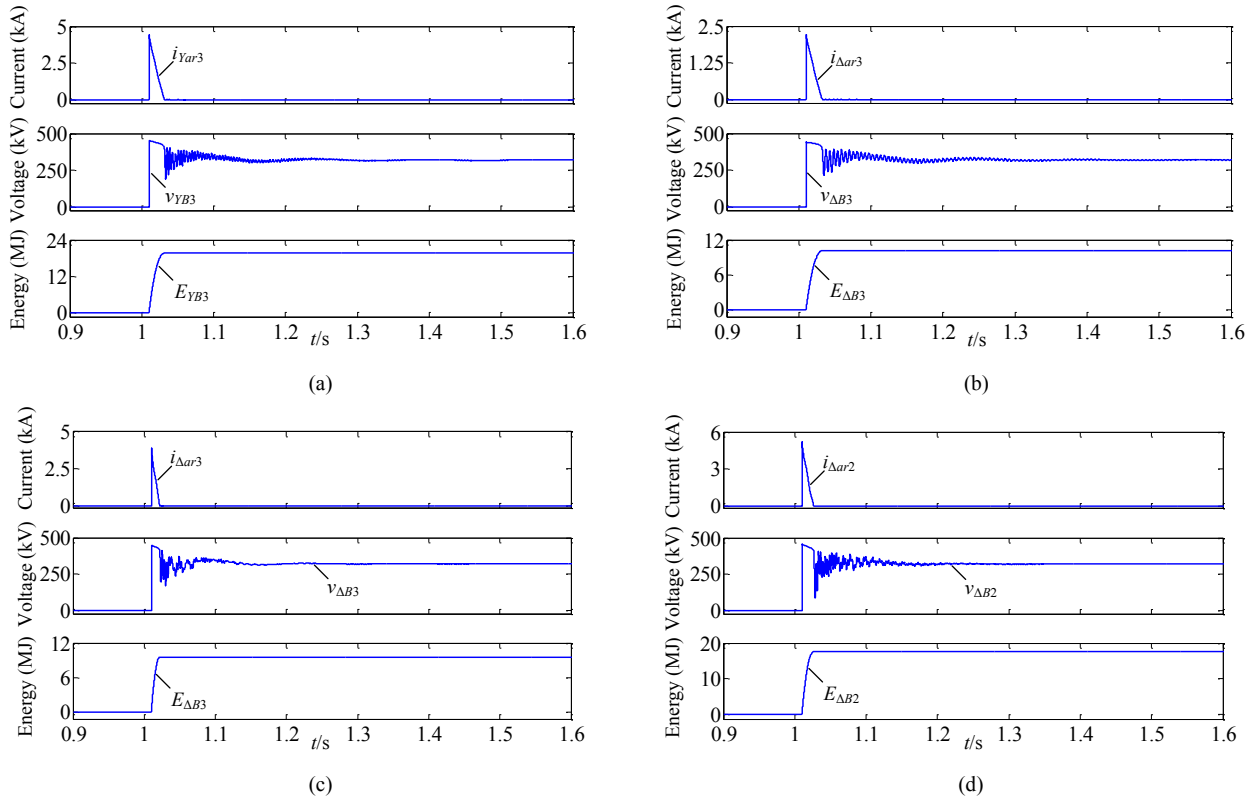


Fig. 8. Currents, voltages, and energies of metal-oxide surge arresters in DCCBs: (a) $B_3$ in star-configuration with DCLs, (b) $B_3$ in delta-configuration with external DCLs, (c) $B_3$ and (d) $B_2$ in delta-configuration with internal DCLs.

The DCCB is modelled as a mechanical switch with an opening time of 10 ms and a metal-oxide surge arrester connected in parallel to protect the DCCB against over-voltages [20]. Fig. 8 shows the current, voltage and energy of the metal-oxide surge arrestors. Once the mechanical switch opens at $t_1$=1.01 s, the current through the switch is commutated into the surge arrestor to limit the voltages across the DCCB, without exposing it to significant over-voltage. As the protection voltages of the surge arresters are all set at 1.5 pu, the proposed fault protection structures in Fig. 6 have similar surge arrester voltage stresses with that in [27] and the absorbed energies are mainly determined by the DCCB currents. In the DCL star-configuration, only circuit breaker $B_3$ opens at $t_1$=1.01 s while $B_1$ and $B_2$ continue to transfer power between stations $S_1$ and $S_2$. As a result, the voltages of surge arrestors in $B_1$ and $B_2$ are around zero and they do not absorb energy during the fault. All the opening energy is absorbed by the surge arrestor in $B_3$ and this energy reaches 19.6 MJ, as shown in Fig. 8 (a).

For the delta-configuration with external inductors, $B_2$ and $B_3$ open to isolate the fault and the energy is shared equally between their surge arrestors. As shown in Fig. 8 (b), the current peak and energy are reduced to 2.2 kA and 10.1 MJ respectively, half that of DCL star-configuration. The capacity of the proposed delta DCCB configuration is reduced dramatically.

 

When the inductors are connected inside the delta-configuration, the energies absorbed by $B_3$ and $B_2$ are no longer equal and reach 9.5 MJ and 17.5 MJ respectively, as depicted in Fig. 8 (c) and (d). Their sum is larger than that of star-configuration and delta-configuration with external DCLs, due to the lower short-circuit impedance at the DC-link node and larger fault currents.

## IV. Performance Evaluation of DC Fault Tolerant Operation

### *A. Delta-Configuration with External DC Inductances*

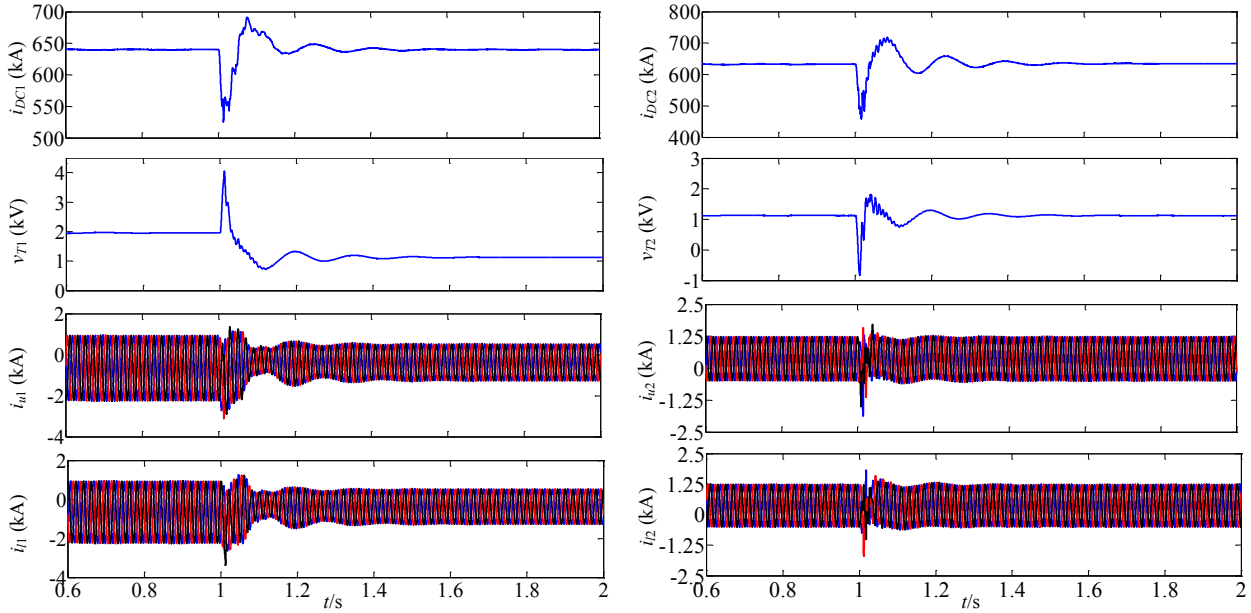


Fig. 9. DC fault tolerant operation waveforms of delta-configuration with external DCLs: (a) DC voltage, DC current, upper arm currents, and lower arm currents of station $S_1$ and (b) DC voltage, DC current, upper arm currents, and lower arm currents of station $S_2$.

The continuous operation of healthy system parts in the event of a DC fault at one DC branch is assessed using the radial three-terminal HVDC model shown in Fig. 1 and Table I. The simulated scenarios are identical to those discussed in Section III B. The delta-configuration with external DCLs shown in Fig. 6 (a) is connected at the DC-link node to delay and isolate the fault propagation and the inductances are 500 mH. The results are shown in Fig. 9.

By virtue of the protection structure at DC-link node, the minimum DC voltage of $S_1$ is increased to 525 kV whilst the fault arm current peak is reduced to 3.4 kA, lower than the 4 kA threshold, Fig. 9 (a). The peak of fault arm current in station $S_2$ is around 1.8 kA and lower than that of $S_1$, due to its larger short-circuit impedance and lower initial current, Fig. 9 (b).

The DC current of $S_1$ increases after the fault and reaches the peak of around 4 kA. Differently, the DC current of $S_2$ needs to change direction and reaches a maximum of 1.8 kA during the restoration period. The different fault DC

 

current behaviours in $S_1$ and $S_2$ depend on the power direction. As station $S_3$ is isolated from the healthy parts by breakers $B_2$ and $B_3$, the steady state DC current of $S_1$ is reduced from 1.9 kA to 1.1 kA after the fault, which is identical to that of $S_2$.

### *B. Consideration of DC Inductance Size*

For the delta-configuration with external 500 mH inductance, the fault arm current is limited to 3.4 kA, as shown in Fig. 9. When the DC inductance is reduced to 380 mH, the fault arm current is slightly lower than the threshold limit of 4 kA. Another reason for requiring relatively large additional DC inductances is the long opening time of the DCCB (10 ms) considered in this paper. If the DCCB has a 5 ms opening time as in [29] and [30], the DC inductance can be reduced from 380 mH to 140 mH. Further, if hybrid DCCBs with 2 ms opening time as suggested in [31, 32] are used, the DC inductance is reduced from 140 mH to 50 mH. These factors reduce the DC inductance significantly, which makes the proposed scheme more applicable to potential offshore HVDC projects where the volume and weight restrictions for the DC reactors are critical, if placed on an offshore platform.

## V. CONCLUSION

This paper proposes the delta-configuration of DCCBs combined with additional DC inductances, for the inter-connection of HVDC systems. The DCCB losses are reduced by the proposed delta-configuration, being 33.3% of those with the conventional star-configuration. During the fault, the current and energy stresses experienced by DCCBs with the delta-configuration are reduced dramatically and the DCCB capacities are only half those of a star-connection. By using the proposed delta-configuration, power can continue to be transferred among the three-terminals through the healthy circuit breakers, in the event of a DCCB being out of service, benefiting from parallel paths. Therefore the proposed delta-configuration is tolerant to DCCBs being out of service, yielding high reliability. By combining the proposed DCCB delta-configuration with DC inductances at the DC-link node, continuous operation of the healthy part of the HVDC network is ensured during (system ride through) and after a DC fault. The proposed DCCB delta-configuration and the protection structures provide an attractive approach with low power loss and cost, and offer discrimination, robustness and increased system availability for applications in future multi-terminal HVDC systems.

## ACKNOWLEDGEMENT

This research was support by EPSRC grants EP/K006428 and EP/K035096, and NSFC grant 51261130484.

## VI. REFERENCES

[1] Z. Rong, X. Lie, Y. Liangzhong, and B. W. Williams, "Design and Operation of a Hybrid Modular Multilevel Converter," *IEEE Trans. Power Electron.,* vol. 30, pp. 1137-1146, 2015.

[2] M. K. Bucher, M. M. Walter, M. Pfeiffer, and C. M. Franck, "Options for ground fault clearance in HVDC offshore networks," in *Energy Conversion Congress and Exposition (ECCE), 2012 IEEE*, 2012, pp. 2880-2887.

[3] M. Firouzi and G. Gharehpetian, "Improving fault ride-through capability of fixed-speed wind turbine by using bridge-type fault current limiter," *IEEE Trans. Energy Convers,* vol. 28, pp. 361-369, 2013.

[4] R. Li, G. Adam, D. Holliday, J. Fletcher, and B. Williams, "Hybrid Cascaded Modular Multilevel Converter with DC Fault Ride-Through Capability for HVDC Transmission System," *IEEE Trans. Power Del.,* vol. PP, pp. 1-1, 2015.

[5] J. Descloux, P. Rault, S. Nguefeu, J. B. CURIS, X. Guillaud, F. Colas*, et al.*, "HVDC meshed grid: Control and protection of a multi-terminal HVDC system," *CIGRE,* 2012.

[6] T. Lianxiang and O. Boon-Teck, "Protection of VSC-multi-terminal HVDC against DC faults," in *Power Electronics Specialists Conference, 2002. pesc 02. 2002 IEEE 33rd Annual*, 2002, pp. 719-724 vol.2.

[7] C. Meyer, M. Kowal, and R. W. De Doncker, "Circuit breaker concepts for future high-power DC-applications," in *Industry Applications Conference, 2005. Fourtieth IAS Annual Meeting. Conference Record of the 2005*, 2005, pp. 860-866 Vol. 2.

[8] I. A. Gowaid, G. P. Adam, A. M. Massoud, S. Ahmed, D. Holliday, and B. W. Williams, "Quasi Two-Level Operation of Modular Multilevel Converter for Use in a High-Power DC Transformer With DC Fault Isolation Capability," *IEEE Trans. Power Electron.,* vol. 30, pp. 108-123, 2015.

[9] E. Kontos, R. T. Pinto, S. Rodrigues, and P. Bauer, "Impact of HVDC Transmission System Topology on Multiterminal DC Network Faults," *IEEE Trans. Power Del.,* vol. PP, pp. 1-1, 2014.

[10] J. Peralta, H. Saad, S. Dennetiere, J. Mahseredjian, and S. Nguefeu, "Detailed and Averaged Models for a 401-Level MMC–HVDC System," *IEEE Trans. Power Del.,* vol. 27, pp. 1501-1508, 2012.

[11] H. Saad, J. Peralta, S. Dennetiere, J. Mahseredjian, J. Jatskevich, J. A. Martinez*, et al.*, "Dynamic Averaged and Simplified Models for MMC-Based HVDC Transmission Systems," *IEEE Trans. Power Del.,* vol. 28, pp. 1723-1730, 2013.

[12] S. Tasnim, A. Rahman, A. M. T. Oo, and M. F. Islam, "Power losses from wind generated electricity in high voltage AC transmission: an analysis through simulation," *International Journal of Renewable Energy Technology,* vol. 5, pp. 77-92, 2014.

[13] R. Li, J. E. Fletcher, L. Xu, D. Holliday, and B. W. Williams, "A Hybrid Modular Multilevel Converter with Novel Three-level Cells for DC Fault Blocking Capability," *IEEE Trans. Power Del.,* vol. PP, pp. 1-1, 2015.

[14] R. T. Pinto, P. Bauer, S. F. Rodrigues, E. J. Wiggelinkhuizen, J. Pierik, and B. Ferreira, "A Novel Distributed Direct-Voltage Control Strategy for Grid Integration of Offshore Wind Energy Systems Through MTDC Network," *IEEE Trans. Ind. Electron.,* vol. 60, pp. 2429-2441, 2013.

[15] R. Marquardt, "Modular Multilevel Converter topologies with DC-Short circuit current limitation," in *Power Electronics and ECCE Asia (ICPE & ECCE), 2011 IEEE 8th International Conference on*, 2011, pp. 1425-1431.

[16] T. Lianxiang and O. Boon-Teck, "Locating and Isolating DC Faults in Multi-Terminal DC Systems," *IEEE Trans. Power Del.,* vol. 22, pp. 1877-1884, 2007.

[17] Z. Shi, Y. Zhang, S. Jia, X. Song, L. Wang, and M. Chen, "Design and numerical investigation of A HVDC vacuum switch based on artificial current zero," *Dielectrics and Electrical Insulation, IEEE Transactions on,* vol. 22, pp. 135-141, 2015.

[18] L.-E. Juhlin, "Fast breaker failure detection for HVDC circuit breakers," ed: Google Patents, 2015.

[19] P. Jae-Do, J. Candelaria, M. Liuyan, and K. Dunn, "DC Ring-Bus Microgrid Fault Protection and Identification of Fault Location," *IEEE Trans. Power Del.,* vol. 28, pp. 2574-2584, 2013.

[20] J. Magnusson, R. Saers, L. Liljestrand, and G. Engdahl, "Separation of the Energy Absorption and Overvoltage Protection in Solid-State Breakers by the Use of Parallel Varistors," *IEEE Trans. Power Electron.,* vol. 29, pp. 2715-2722, 2014.

[21] V. Vita, A. D. Mitropoulou, L. Ekonomou, S. Panetsos, and I. A. Stathopulos, "Comparison of metal-oxide surge arresters circuit models and implementation on high-voltage transmission lines of the Hellenic network," *Generation, Transmission & Distribution, IET,* vol. 4, pp. 846-853, 2010.

[22] Z. J. Shen, G. Sabui, Z. Miao, and Z. Shuai, "Wide-Bandgap Solid-State Circuit Breakers for DC Power Systems: Device and Circuit Considerations," *Electron Devices, IEEE Transactions on,* vol. 62, pp. 294-300, 2015.

[23] K. Sano and M. Takasaki, "A Surgeless Solid-State DC Circuit Breaker for Voltage-Source-Converter-Based HVDC Systems," *Industry Applications, IEEE Transactions on,* vol. 50, pp. 2690-2699, 2014.

[24] F. Dijkhuizen and B. Berggren, "Zoning in High Voltage DC (HVDC) Grids using Hybrid DC breaker," in *EPRI HVDC and FACTS Conferences, USA*, 2013.

[25] R. Derakhshanfar, T. Jonsson, U. Steiger, and M. Habert, "Hybrid HVDC breaker–Technology and applications in point-to-point connections and DC grids," in *CIGRE Session*, 2014, pp. 1-11.

[26] M. Callavik, A. Blomberg, J. Häfner, and B. Jacobson, "The Hybrid HVDC Breaker-An innovation breakthrough enabling reliable HVDC grids," *ABB Grid Systems, Technical paper Nov,* 2012.

[27] G. Adam, R. Li, D. Holliday, S. Finney, L. Xu, B. Williams, *et al.*, "Continued Operation of Multi-Terminal HVDC Networks Based on Modular Multilevel Converters," *CIGRE,* pp. 1-8, 2015.

[28] Y. Jin, J. E. Fletcher, and J. O'Reilly, "Short-Circuit and Ground Fault Analyses and Location in VSC-Based DC Network Cables," *IEEE Trans. Ind. Electron.,* vol. 59, pp. 3827-3837, 2012.

[29] T. Eriksson, M. Backman, and S. Halen, "A low loss mechanical HVDC breaker for HVDC Grid applications," *Proc. Cigré Session, Paris, France,* 2014.

[30] K. Tahata, S. Ka, S. Tokoyoda, K. Kamei, K. Kikuchi, D. Yoshida, *et al.*, "HVDC circuit breakers for HVDC grid applications," in *Proc. Cigré AORC Technical Meeting, Tokyo, Japan*, 2014.

[31] E. Kontos, R. T. Pinto, S. Rodrigues, and P. Bauer, "Impact of HVDC Transmission System Topology on Multiterminal DC Network Faults," *IEEE Trans. Power Del.,* vol. 30, pp. 844-852, 2015.

[32] M. Hajian, D. Jovcic, and W. Bin, "Evaluation of Semiconductor Based Methods for Fault Isolation on High Voltage DC Grids," *Smart Grid, IEEE Transactions on,* vol. 4, pp. 1171-1179, 2013.